Differential remodelling in small and large murine airways revealed by novel whole lung airway analysis.

Amanda L Tatler[1+], Christopher J Philp[1+], Michael R Hill[2+], Sam Cox[3], Andrew Bullock[2], Anthony Habgood[1], Alison John[1], Robert Middlewick[1], Katherine E Stephenson[1], Amanda T Goodwin[1], Charlotte K Billington[1], Reuben D O'Dea[2], Simon R Johnson[1#], Bindi S Brook[2#*].

1. Centre for Respiratory Research, NIHR Biomedical Research Centre and Biodiscovery Institute, School of Medicine, University of Nottingham.
2. School of Mathematical Sciences, University of Nottingham.
3. Digital Research Service, University of Nottingham.

+ First authors contributed equally to this manuscript
 # Joint senior author

** Address correspondence to*: Bindi S. Brook; bindi.brook@nottingham.ac.uk;
Tel: +44 (0)115 748605.

Running Head:
Whole lung airway analysis

Online supplementary methods and results: https://doi.org/10.6084/m9.figshare.19085786.v1

Acknowledgements:
This study was funded by the Medical Research Council (MRC), Grant Number MR/M004643/1. ALT was funded by a Medical Research Foundation/Asthma UK mid-career fellowship during this work (grant number MRFAUK-2015-312)

Contributions:
Experimental work: CJP, CKB, ALT, AH, AEJ, RM, KES, ATG
Conception and design of the study: CJP, MRH, CKB, ALT, RDO, BSB, SRJ
Analysis and interpretation: CJP, MRH, CKB, ALT, RDO, BSB, SRJ
Image analysis computational code: MRH, AB, SC, RDO, BSB
Drafting the manuscript for important intellectual content: CJP, MRH, CKB, AB, ALT, RDO, BSB, SRJ
ALT, CJP and MRH performed the animal work, airway analysis and mathematical analysis respectively, giving equal contributions to the work.

Competing interests statement:
SRJ received research funding from Pfizer, outside the submitted work. None of the authors have competing interests.

Abstract

Airway remodelling occurs in chronic asthma leading to increased airway smooth muscle (ASM) mass and extra-cellular matrix (ECM) deposition. Whilst extensively studied in murine airways, studies report only selected larger airways at one time point meaning the spatial distribution and resolution of remodelling are poorly understood. Here we use a new method allowing comprehensive assessment of the spatial and temporal changes in ASM, ECM and epithelium in large numbers of murine airways after allergen challenge. Using image processing to analyse 20-50 airways per mouse from a whole lung section revealed increases in ASM and ECM after allergen challenge were greater in small and large rather than intermediate airways. ASM predominantly accumulated adjacent to the basement membrane whereas ECM was distributed across the airway wall. Epithelial hyperplasia was most marked in small and intermediate airways. Post challenge, ASM changes resolved over seven days whereas ECM and epithelial changes persisted. The new method suggests large and small airways remodel differently and the long-term consequences of airway inflammation may depend more on ECM and epithelial changes than ASM. The improved quantity and quality of unbiased data provided by the method reveals important spatial differences in remodelling and could set new analysis standards for murine asthma models.

Introduction

Asthma is a chronic disease characterised by airway inflammation, hyperresponsiveness and episodes of airway narrowing. Inflammatory events cause the recruitment and activation of eosinophils, mast cells and T- cells, which generate mediators and growth factors amplifying airway inflammation. Bronchoconstrictor stimuli cause acute airway narrowing and additionally promote ASM growth. Repeated episodes of inflammation and bronchoconstriction induce a series of long-term structural changes, comprising increased airway smooth muscle (ASM) mass, extra-cellular matrix (ECM) deposition and epithelial metaplasia, collectively termed airway remodelling. This process results in fixed airway narrowing, increased need for medication and worsening outcomes for people with asthma. Crucially, severe airway remodelling is associated with lung function decline (1).

Physiologic and, more recently, imaging studies have shown that airway remodelling varies with airway size and these differential changes may have important long-term physiologic impacts (2-5). Obtaining tissue samples to study airway remodelling in humans is invasive and generally provides only small tissue samples from large airways at one or two timepoints from which it is difficult to infer whole organ function. Models using repeated airway challenge in sensitised animals are therefore frequently used to understand the mechanisms underlying airway remodelling (6). In the past 10 years, there have been over 1100 primary research articles using mice to study airway remodelling which at a conservative estimate equates to 22 000 animals (PubMed search December 2022 - ((airway remodelling) AND mouse) AND model AND asthma. Animal calculation assumes 20 animals used per study i.e. two groups of 10 animals). Somewhat surprisingly, despite the large number of animals used, there is no consensus on experimental methodology used, nor the type and quality of data reported, and the number of animals with the size of airways analysed are frequently not reported. At best this means that animal tissue is not used to its full advantage and potentially that in some cases a small number of unrepresentative airways are selected, biased by appearance and size. Such methodology

also fails to account for, or characterise, intra-subject heterogeneity which is likely to be an important determinant of function at the organ level (7) .

Here we set out to develop a methodology which allows us to examine airway remodelling and resolution across the whole range of airways in murine lungs. We hypothesised that this novel approach would reduce selection bias and provide hitherto hidden information on differential structural effects of airway remodelling across airway sizes. Furthermore, by extracting richer data, more information could be obtained from fewer animals and so our method contributes to improving data collection standards for both comprehensively assessing airway remodelling and minimising animal use (8-12).

Methods

Study approval

Animal work was approved by the Animal Welfare and Ethical Review Board (AWERB) of the University of Nottingham (UK) and conducted in accordance with all terms of the Establishment, Project and Personal Licenses issued by the Secretary of State for the Home Office. Consistent with all national and international law, studies were carried out as detailed in the Animal [Scientific Procedures] Act 1986 (Amended Regulations 2012) (ASPA), Animal Welfare Act 2006, Directive 2010/63/EU, the LASA guidelines and in respect to the principals of Replacement, Reduction and Refinement. Work was performed under project (PPL) license number RGJ 40/3709 using the 19b5 protocol.

Animals and Tissue Processing

Ten 6-week old female BALB/C mice underwent ovalbumin (OVA) sensitisation on two occasions 10 days apart. Ten OVA airway challenges were performed between days 17 and 33 as previously described (13). Control animals were sensitised but challenged with phosphate buffered saline (PBS; Sigma Aldrich, UK). Animals were randomised to either the OVA or control challenge groups. OVA-challenged animals were sacrificed by anaesthetic overdose at day 34, 24 hours after the final inhaled challenge, which was defined as maximal remodelling, and at days 35, 37, 39 and 41 to track resolution (Fig 1A). Control animals were sacrificed at days 34 and 41 only. Group numbers at each timepoint are given in Table 1. For each animal, the trachea was cannulated and bronchoalveolar (BAL) lavage performed using 1ml of chilled sterile PBS. The BAL fluid (BALF) was centrifuged at 1500rpm (4°C) for 10 minutes and the supernatant removed. The pelleted inflammatory cells were resuspended in 1ml sterile PBS, and 200µl of the cell suspension was placed in a Cytofunnel™ (Thermo Fisher, UK) and centrifuged at 450rpm for 6 minutes. The cytospun cells were stained using Rapi-Diff staining kit following manufacturer's instructions. Slides were visualised using a Nikon Eclipse 90i microscope and

the percentage of macrophages, eosinophils, neutrophils and lymphocytes counted by an observer blind to the animal's treatment.

The lungs were inflated at 20cm/H2O with 4% formaldehyde and the whole respiratory tract paraffin wax embedded *en block* (Fig 1B). Lung samples were sectioned through their coronal axis (Fig 1B) using the centre of the trachea and bronchi as a means of ensuring equivalent sectioning across samples. Sequential sections were stained for α-smooth muscle actin (SMA) by immunohistochemistry and picrosirius red (PSR) as previously described (14) and in supplemental methods. The former stain allows quantification of ASM distribution; the latter stains predominantly for collagen, the main deposited protein within the ECM and so for brevity is referred to as ECM henceforth. Whole slide images were then captured with a Digital Nanozoomer (Hamamatsu Photonics UK), converted to tiff format at maximum resolution using ndpi2tiff (https://www.imnc.in2p3.fr/pagesperso/deroulers/software/ndpitools/) and imported into MATLAB (The Mathworks Inc) for processing. The custom image analysis software developed in MATLAB is described below (and can be downloaded from: https://github.com/BindiBrook/AirwayIdentification); full details are given in the online supplement.

MATLAB Workflow and Program Design

A custom pre-processor was developed in MATLAB to identify potential airways, which were then filtered to keep objects with characteristics associated with airways and eliminate those without. Full details and code are provided in the on-line supplement and at: https://github.com/BindiBrook/AirwayIdentification respectively. Briefly, irregular circular objects were identified via a multi-step process and converted to a binary image. Epithelial breaks were closed, the lumen identified, smoothed and areas calculated. Minimum and maximum effective diameters were set between 25 and 500 μm, with objects outside the selected range eliminated in order to avoid

including cross-sections smaller than alveoli (15) and as large as the main bronchi (16). The perimeter of the trace and the area bounded were computed and objects with pre-defined area-perimeter ratios chosen as potential airways (Fig 1C). A custom filtering algorithm, based upon the airway shape regularity and wall density was used to determine airways from other objects such as blood vessels or alveoli. A script then allowed visualisation of the filtered images for manual review and editing. Objects that were classified as "rejected airways" were also retained for full user checking if required.

Airway Analysis and Quantification

After airway identification the outer boundary of the epithelium, representing the basement membrane was traced manually for every airway (Fig 1D). The script then automatically placed a second boundary to define the airway wall by dilating the region bounded by the basement membrane by 40 μm; manual alterations to this boundary can be made by the user if necessary. This uniform airway wall thickness was chosen to provide a simple and consistent way to ensure that all airway features are accommodated, without including excessive lung parenchyma, and avoided difficulties associated with identifying the outer boundary of the airway wall automatically. SMA or PSR positivity was quantified by threshold setting of stained pixels within the airway objects. Separate user-defined thresholds were employed for SMA and PSR staining. Total airway area fractions of ASM and ECM were computed as the ratio of the area of SMA or PSR positive pixels respectively, relative to the total area within the basement membrane and second boundary. Spatial distributions across the airway wall thickness were determined similarly, by the ratio of the area of SMA or PSR pixels occurring within a narrow 'annulus' between two radial spatial positions, and the total within that region, with these regions being obtained via the dilation process as above (Fig 1E). Lumen area and 'inner area' (the area contained within the basement membrane outline) are determined by pixel count, as above; epithelial area was determined by subtracting the lumen area from the inner area in the SMA-stained airway images (Supp Fig 5A). Subsequent analysis of airway composition (see the online supplement for detail) indicated that the choice of fixed airway thickness described above did not influence our results.

Data Analysis and Statistics

Data analysis and statistics were performed using custom scripts in MATLAB. The complete datasets are available at this link: https://uniofnottm-my.sharepoint.com/:f:/g/personal/bindi_brook_nottingham_ac_uk/EuO4q5619NZNrTyhuo2IUaUBvRmQFcIA8WoKhXmckOddcg?e=iC7qHb

Results

At the end of the 34-day sensitisation and challenge protocol, in the saline challenged control mice macrophages comprised 99% (SEM±0.5) of BAL cells. Chronic OVA challenge was associated with an increase in BAL eosinophils (43±3.5%), lymphocytes (13±1.6%), neutrophils (4±0.9%) and a relative reduction in macrophages (40±3.6%). These changes progressively and completely resolved over seven days following the cessation of airway OVA-challenge (Fig 2A).

Global changes in airway smooth muscle and collagen

The protocol identified a total of 1007 PSR-stained and 1022 SMA-stained airways across all 28 control and 58 OVA-challenged animals over 5 timepoints. At each timepoint we identified 90-240 airways from 4-10 mice (see Table 1 for breakdown). ECM and ASM area fractions were calculated for each airway (Supplementary Table 1).

Mean ASM area fraction in OVA-challenged animals, observed at day 34, was significantly greater than in control animals (Fig 2B, left panel; one-way ANOVA, $p = 0.0353$). Elevated ASM area fraction in OVA conditions at day 34 resolved rapidly, with no significant difference in mean area fraction to day 34 control observed over the seven-day resolution period, returning almost to baseline by day 41. The variability in ASM area fraction associated with remodelling also decreased to similar levels to control animals by day 41 in all but those airways with the highest ASM fraction (Figs 2B, right panel; and 2C).

In contrast to ASM, the observed increase in mean ECM area fraction at day 34 was not significant (compared to control) but remained elevated after cessation of airway challenge, with statistically significant increases observed at days 37, 39, and 41 compared to control (Fig 2B, left panel; one-way ANOVA, $p = 0.0292$, 0.0183, 0.0140 respectively). The increased variability in the ECM area fraction associated with remodelling was also sustained (Figs 2B, right panel, and 2C). Additionally, ECM fraction increased 1.3-fold in control animals between day 34 and 41 although these changes were smaller than those due to OVA challenge-associated remodelling.

198 The trends in data are more readily observable in the pooled data (Fig 2B, right panel), in which every
199 point represents an airway, showing the large increase in ASM fraction at day 34 which resolves
200 rapidly, while the ECM increase appears to occur over a slower timescale and remains elevated during
201 the resolution period.
202
203 The full distribution of area fraction data obtained within each group at day 34 is shown in Figure 2C
204 left panel, highlighting the rich information on intra-subject heterogeneity in our dataset (see also
205 Supplementary Fig 3). On day 34, the right shift in distribution peak shows increases in ASM and ECM
206 area fractions (statistical significance discussed above) in OVA-challenged when compared with control
207 animals. Additionally, the heterogeneity of ECM and ASM remodelling (as highlighted by the width of
208 the distributions) differed from control airways with a 1.3- and 1.5-fold increase in variance
209 respectively (Fig 2C).

210 *Stratification of remodelling changes by airway size*

211 It is well established that remodelling is a response to both inflammatory mediators and the micro-
212 mechanical environment of resident cells and ECM (17-21). The emergent remodelling response
213 determined by this complex, multiscale system will therefore depend sensitively on small differences
214 in, for example, local inflammatory response, airway geometry, and mechanical properties at the
215 airway and cellular level (22-30). Therefore, in what follows we exploit our entire dataset to examine
216 the pattern and time course of remodelling and resolution across airways of different sizes for the first
217 time.

218 The methodology allows detailed measurement of additional airway parameters including lumen area
219 and basement membrane (BM) perimeter. Airways were initially arbitrarily divided into small (BM
220 perimeter <500μm), medium (501μm-1000μm) and large (1001μm-1500μm) categories. To allow
221 direct comparisons between airways stratified by size, we first determined that neither the range nor
222 the mean of the distribution of BM perimeters differed between control and OVA-challenged animals

223 at day 34 (one-way ANOVA, p= 0.166 and two-sample KS tests, p=0.08 respectively). At day 41 mean
224 BM perimeter did not differ significantly (one-way ANOVA, p=0.166), although the distribution of these
225 changes did vary somewhat (two-sample KS tests p=0.0069). At day 41 mean BM perimeter did not
226 differ significantly (one-way ANOVA, p=0.166), although the distribution of these changes did vary
227 somewhat (two-sample KS tests p=0.0069).

228 In OVA-challenged animals at maximal remodelling on day 34, mean ECM area fraction increased
229 significantly in small and medium sized airways by 1.7 and 1.4-fold respectively compared with control
230 animals. A 1.3-fold increase in large airways was not significant (Fig 3A); p-values corresponding to
231 these statistical tests, and those described below, are given in the relevant panels of Figure 3. ECM
232 remodelling in each category was sustained over the post-challenge period to day 41 with 1.9, 1.5 and
233 1.4-fold increases respectively, compared with control at day 34 (Fig 3A). Mean ASM area fraction also
234 increased at day 34 in all airway sizes, although the pattern of remodelling differed with the greatest
235 increase in large airways; 1.8, 1.5 and 1.9-fold increases were observed in small, medium and large
236 airways, respectively (Fig 3B). The mean ASM area fraction at day 41 had fallen to control levels in
237 medium and large but not small airways; however, only a relatively small number of airways could be
238 identified in this group (Fig 3B). ASM remodelling resolved to a greater degree in large and small rather
239 than medium-sized airways (Fig 3B, middle column) and is consistent with the wider distribution of
240 ASM fractions at day 41 in the OVA-challenged animals (Fig 2B).

241 *Fine stratification by airway size*

242 These airway size categories are a convenient way to observe differential airway remodelling and
243 highlight how the distributions within each airway range informs their interpretation. However, our
244 dataset allows us to examine the heterogeneity in airway remodelling in finer detail by considering the
245 relationship between ASM and ECM fractions across the whole range of airway sizes (defined by
246 basement membrane perimeter). As BM perimeter distributions do not differ between control and
247 OVA-challenged animals at day 34, the remodelling observed can largely be attributed to increased

248 airway ASM and ECM content. 3D histograms that show the frequency of observed airway area
249 fraction split across finely-resolved size categories, show that ECM and ASM distributions are more
250 diffuse in OVA-challenged compared with control animals, consistent with the increased variance seen
251 with airway size stratification (Fig 4A). Comparison between the orientation of the distribution peaks in
252 control and OVA-challenge conditions, shown by lines of best fit (Fig 4B,C and Supplementary Figure 4)
253 highlight the airway size-dependence of remodelling in more granular detail. Uniform remodelling
254 across airway sizes would result in approximately parallel best fit lines in control and challenge
255 conditions, while clockwise or anticlockwise rotation would be associated with increased remodelling
256 in smaller or larger airways, respectively. Consistent with our findings based on coarse stratification,
257 we observe that ECM remodelling decreases progressively with increasing airway size, with little to no
258 remodelling observed in airways with BM perimeter greater than 1000μm. For ASM distributions,
259 however, there is a substantial change in peak orientation, corresponding to increased remodelling in
260 small compared with larger airways (with BM greater than approximately 750μm), although the small
261 number of large airways means that the linear correlation lines should be interpreted with care in the
262 latter region. The resolution of remodelling in both ECM and ASM, shows substantial variation over the
263 seven-day post-challenge period highlighted by tracking the location of mean ECM and ASM from the
264 2D projections over all time points (Supp Fig 4E-H). This emphasises the contrast in the overall trend
265 for ASM content to resolve to almost control levels, while ECM continues to remodel throughout this
266 period.
267
268 *Spatial distributions of ASM and ECM across the airway wall*

269 We next examined how total area fraction of ASM and ECM were distributed radially from the
270 basement membrane to the outer airway margin (Fig 1D,E), and how this changed during remodelling
271 (Fig 5). In control animals at day 34 and 41, ECM content was highest in the 40% of the airway adjacent
272 to the basement membrane, peaking at 20% in each case (blue and yellow curves, Fig 5A, left column;
273 Fig 5C, left panel). In contrast, increased ECM content in control animals at day 41 was restricted to the

30% of the airway wall adjacent to the basement membrane, with little or no increase elsewhere. ECM remodelling in OVA-challenged animals at day 34 followed a similar pattern, but with a shift in the peak location towards the airway wall mid-point (Fig 5A, top right panel) and increased ECM deposition in the outer 80% of the airway compared with control at day 34 (cf. blue and orange curves in Fig 5A, top row and Fig 5C, left panel). The increased ECM observed in outer regions of the airways in OVA-challenged animals at day 34 is maintained during the post-challenge phase until day 41 (cf. orange and purple curves in Fig 5A and Fig 5C, left panel). Further increases in ECM content occurred in the 40% of the airway adjacent to the basement membrane and, interestingly, the location of the peak in the OVA-treated animals shifted back towards the basement membrane, as exhibited by the control data (cf. purple and yellow curves in Fig 5C, left panel). ASM content in control animals was also highest in the 40% of the airway thickness nearest the basement membrane, peaking at 20% with very little ASM more peripherally (Fig 5B, left column). OVA challenge resulted in increased ASM content in the region 20-80% from the basement membrane, with a shift in the peak further away from the basement membrane (cf. blue and orange curves in Fig 5B, top row and Fig 5C, right panel). Over the post-challenge period, the peak and overall distribution returned close to control levels (cf. purple and yellow/blue curves; Fig 5C, right panel).

The comprehensive dataset, shown in Figs 4 and 5A,B, also highlights the heterogeneity in airway composition both in control and post-challenge conditions. We further investigate this in Supplementary Figure 3, demonstrating wide variation in total ECM area fraction and its radial variation between animals, but with somewhat more consistent response observed in OVA-challenge conditions compared to control. Additionally, BM perimeter shows greater consistency between animals than does airway constituent remodelling.

Epithelial involvement in remodelling

298 To determine how the epithelial layer was affected by remodelling (Fig 6) we computed the epithelial
299 area for each airway as shown in Supplementary Figure 5A. To correct for airway size, the epithelial
300 area between the BM and airway lumen was normalised to the BM perimeter so that we obtain a
301 measurement of epithelial area per unit BM perimeter length. For concision, we refer to this as
302 'normalised epithelial area' below. For 550 airways examined at days 34 and 41, the mean normalised
303 epithelial area was higher in ovalbumin-challenged compared with control animals as indicated by the
304 right shift in distribution peaks, as was the variability, indicated by the width of the distributions (Fig
305 6A). In the 28 control and 58 OVA-challenged animals over 5 timepoints, the mean normalised
306 epithelial area was significantly increased at day 34 (n= 6 mice; p = 0.0025) compared with control at
307 day 34 (n = 6 mice) and remained elevated at all subsequent timepoints (p = 0.012, 0.0035, 0.0053,
308 0.0188; n = 6, 8, 6, 4, 10 respectively; Fig 6B) with fold-increase ranging from 1.38 – 1.44. Stratification
309 by size shows that the changes at day 34 were driven by large (1.7-fold; p = 2.4×10^{-8}) and medium
310 sized (1.3-fold; p=1.2×10^{-19}) but not small airways (Fig. 6C,D,). The last observation is also consistent
311 under finer stratification as indicated by the anticlockwise rotation of the line of best fit in the 2D
312 projection of BM perimeter vs normalised epithelial area histograms (Fig 6E) in ova-challenged animals
313 compared with control animals at D34.

314 We expected the observed increase in normalised epithelial area to result in a decrease in normalised
315 lumen area (normalised to BM perimeter, as described above), given that the mean BM perimeter
316 remains largely unchanged. However, the mean normalised lumen area was not significantly altered in
317 OVA-challenged compared to control animals at either day 34 or 41 (one-way ANOVA, p=0.9935,
318 0.0616 respectively). This observation was investigated further using simulations based on day 34
319 control data (Fig 7), together with simplified geometrical arguments (Supp. Fig 5). The latter provides a
320 mathematical constraint under which, both normalised epithelial and lumen area in OVA-challenged
321 animals can indeed exceed that in control animals. The former provides a demonstration of this as
322 follows. First, we generate a set of virtual airways with normalised lumen and inner (that enclosed by
323 the basement membrane, normalised as above) areas distributed as observed in the control animal

airways at day 34. We then employ a statistical model under which OVA challenges are simulated by applying small random perturbations (with statistical properties corresponding to the observed OVA data) to the virtual control data (effectively mimicking a longitudinal study not possible in real animals). The corresponding synthetic normalised epithelial area is computed from their difference. Full details are given in the Supplementary material. Simulated normalised lumen and inner area distributions of course have similar shapes to that of the observed experimental data in OVA-challenged animals at day 34 (cf. green and orange curves in Figs 7A,B, left column; note that the distribution amplitude is not expected to be similar, since these data are directly computed from the control (blue curves)), with similar statistically significant and non-significant increase in means (Figs 7A,B, right column). The corresponding distribution of simulated normalised epithelial area also shows a statistically significant increase in mean and a similar shape to the observed data in OVA-challenged animals at day 34 (Fig 7C); p-values are given in figure panels. Taken together, these data support and explain the unexpected relationship between normalised epithelial area, BM perimeter and normalised lumen area observed in the data.

Discussion

We have developed a new method to examine airway remodelling in mouse whole lung cross-sections. In conjunction with immunohistochemistry, the method allows assessment of the amount and distribution of airway components and can be stratified quantitatively according to airway size. In this study we demonstrate that the method is effective in examining ASM, ECM and epithelial remodelling and for the first time has provided evidence of differential changes in large and small airways in response to chronic airway challenge in mice. Our new technique represents a significant improvement in airway remodelling analysis over conventional methodology. Exploiting image processing techniques, our method permits semi-automatic identification, and detailed quantitative analysis, of significantly larger numbers of airways from the same number of experimental animals than has

hitherto been possible. These extensive datasets support unique insights into airway remodelling processes.

It has long been suggested that remodelling of airways in asthma is not homogeneous and that differential remodelling occurs across airways of varying sizes (31), with a recent report demonstrating clear heterogeneity in airway smooth muscle remodelling (32). The implications of heterogeneous remodelling across larger, proximal and more distal small airways are not fully understood. It has been suggested that remodelling of small airways contributes to airway hyper-responsiveness (33), which is consistent with regional changes in ventilation suggestive of distal airway remodelling (34). Supporting this, small airways significantly contribute to increased total lung resistance in moderate-severe asthma (35). Changes in the distribution and extent of remodelling across airways of varying sizes are also seen between non-fatal and fatal asthma (24) suggesting these observations are clinically important.

The method described here identified profound changes in ASM, ECM and epithelial cell remodelling between airways of varying sizes and demonstrated that distinct features of remodelling do not change in a universal way. Our findings show that small airway remodelling is primarily associated with increases in ASM and ECM fractions whereas epithelial cell remodelling occurs primarily in the larger airways. Increased ASM and ECM mass around small airways in human asthma and animal models has been previously well documented (13, 32, 36-42). However, none of these previously published studies have directly compared ASM and ECM remodelling around small versus large airways. Studies assessing epithelial remodelling in large and small airways are more limited in number; however, Carroll et al. found no significant difference in epithelial damage between large and small airways in human asthma (24). Conversely, Ramos-Barbon et al. have previously demonstrated that increases in ASM mass are greater in small airways compared with large airways (43), which supports our present

findings. Crucially, we have expanded these findings to study both ASM and ECM in the same small and large airways.

Our study shows that the resolution of ASM over the 7-day timescale appears to mirror the resolution of eosinophils which occurs over the same timescale. This has previously not been demonstrated; the only other study that we are aware of in which resolution of inflammatory cells was investigated after cessation of challenge (44) did not include time-points as finely resolved as in our study. Southam and colleagues reported sustained increases in ASM and ECM 4 weeks after cessation of airway challenge (42) whereas our data suggested that ASM mass increases resolve. This difference in finding may be the result of differences in *in vivo* model used; Southam et al used a prolonged house dust mite exposure model that involved 25 frequent airway challenges whereas our model utilised only 10 airway challenges with ovalbumin over a 34 day period.

A strength of the method presented here is the ability to assess features of remodelling across airways of all sizes in an unbiased manner, which has not previously been possible in other studies of airway remodelling. Whilst image analysis methods including stereology are truly unbiased and can capture all structures irrespective of orientation, applying such methods to whole lungs is currently too labour- and data-intensive for most studies. Airway remodelling is primarily assessed using histological and immunohistochemical approaches which, while being excellent methods to study pathological changes in tissues, are prone to many types of selection bias for a number of reasons (45). The ability to scan an entire transverse section of lung tissue, identify every airway present and make multiple measurements within those airways reduces selection and sampling bias. A previous attempt to measure remodelling in airways of all sizes within lung tissue was limited by the dependence on the experimenter to identify airways and draw their boundaries reducing the precision in defining airway size (36). Our system represents a significant advancement in the automatic identification of all airways present and accurate calculation of airway wall dimensions once the basement membrane has been defined manually. This is, to our knowledge, the first automated system for identifying airways within

lung tissue. This model has the potential to set a new, higher standard for the analysis and reporting of airway remodelling changes in animal models of asthma. Indeed, our comprehensive dataset exposes detailed data on intrasubject heterogeneity, which has recently been reported in cases of nonfatal and fatal asthma (32). While reporting data for individual animals is seen as the accepted standard, the large number of airways captured can increase statistical power reducing the number of animals required to appropriately test a hypothesis. Of course, in study design, a balance is required between 3Rs considerations and retaining sufficiently many individual animals and/or airways to demonstrate statistical significance of the phenomenon of interest. Here we have assessed ASM, ECM and epithelial cell remodelling; however, the method allows for a diverse range of measurements to be made, only limited by the availability of a specific immunohistochemical stain, making this a powerful tool to study airway biology and disease.

A second strength of the method presented here is the ability to assess spatial changes in ASM and ECM occurring within the airway. Spatial distributions suggest that although ECM close to the membrane increased in control animals at day 41 compared with control animals at day 34, the more diffuse increase in ECM in the rest of the airway occurs only in OVA-challenged animals and not in control animals. This finding suggests that there is some natural ECM increase near the basement membrane, while the OVA-driven increase is larger and more diffuse. Additionally, we observe that in control animals, areas of higher ECM density appear to correlate with areas of higher ASM density whereas in OVA-challenged animals, increased ECM appears at the outer margins. Taken together, these observations suggest a possible mechanism that warrants further investigation: during airway remodelling increased ASM deposits ECM throughout the airway which then resolves but leaves the ECM behind.

While the method has many advantages there are some limitations. At present the automatic airway identification requires user confirmation that the object identified is an airway, which is somewhat time-consuming. Future work by this group will explore the use of artificial intelligence and machine

learning to classify airways and to segment stained tissue, removing the need for user-dependent airway identification. Finally, due to the nature of the airway identification, only intact airways in cross-section (i.e. a complete circular structure) are identified. This potentially limits the number of airways detected, particularly in sections that have large amounts of tissue artefact due to histological tissue preparation. In this current work we have applied the model to mouse lung tissue. Further validation will explore its utility in human lung tissue.

In summary, we have presented a novel, powerful, semi-automated method that allows detailed, unbiased assessment of airway remodelling changes in the lungs of animals from *in vivo* models of asthma. The method has demonstrated important differences in the spatial remodelling of ECM, ASM and the epithelial layer in airways of various sizes, and key differences in the resolution of such remodelling changes after cessation of airway challenge.

Table 1: Number of mice and airways identified in each group and at each time point.

	ECM (PSR)		**ASM** (aSMA)	
	Number of mice	Number of airways	Number of mice	Number of airways
D34 Control	6	121	6	164
D34 Ova	6	110	6	158
D35 Ova	6	139	6	186
D37 Ova	6	239	8	188
D39 Ova	6	119	6	98
D41 Ova	4	124	4	90
D41 Control	6	155	10	138

Table 2: Number of airways identified in each group stratified by airway size (small (basement membrane perimeter < 500µm), medium (500 – 1000µm) and large (1000 – 1500µm)) at Days 34 and 41.

	ECM (PSR) – Number of airways				**ASM** (aSMA) – Number of airways			
	Day 34		Day 41		Day 34		Day 41	
	Control	Ova	Control	Ova	Control	Ova	Control	Ova
Small	26	17	22	7	25	19	15	5
Medium	68	60	72	54	103	91	90	59
Large	12	21	27	32	22	25	23	15

Legends to figures.

Figure 1: Experimental protocol and data capture. (A) Twelve-week old BALB/C mice underwent ovalbumin (OVA) sensitisation on study days 0 and 10 (grey arrows) followed by 10 ovalbumin airway challenges between days 17 and 33 (black arrows) and were sacrificed on day 34 (maximal remodelling) and days 35, 37, 39 and 41 (white arrows). Control animals were sensitised but challenged with physiological buffered saline (PBS) and sacrificed at days 34 and 41. **(B)** Lungs were wax-embedded en bloc with trachea and bronchi intact. Wax block was dissected in two halves along the coronal plane going through the centre of trachea and bronchi (1). The two halves were butterflied out (2) and serial sections through the lungs in the same plane were then taken (3). **(C)** Whole lung sections were captured using a Hamamatsu Nanozoomer. The software identifies and filters all airway-like objects (indicated with pins) and the user selects the images representing airways from the pool of objects. **(D)** For each airway the user manually traces the basement membrane (BM) (1); the software then draws an outer airway margin (2); the software identifies smooth muscle actin (SMA) or picrosirius red (PSR) stained area which the user confirms or corrects (3) and the software traces the lumen outline (4). **(E)** The spatial distributions of ASM and ECM within the airway are calculated by determining the number of stained pixels within narrow bands between the basement membrane (blue curve) and the band margin (red curve). The number of pixels is averaged over the perimeter of that band and plotted as a function of the normalised radius which places the basement membrane at 0 and the outer airway margin at 1 giving a spatial distribution of stain intensity as shown in the schematic.

Figure 2: Global changes in smooth muscle and extra-cellular matrix during remodelling and resolution (A) Bronchoalveolar lavage cell count. Eosinophils, macrophages, lymphocytes and neutrophils as a percent of total number of cells for both control and ova-challenged animals on days 34 and 41 and for ova-challenged animals on days 35, 37 and 39. **(B)** Global changes in airway

constituents during resolution. Box plots show change in area fraction of ECM (top) and ASM (bottom) between days 34 and 41, for mice as experimental units (left) and airways as experimental units (right). Box plots show the median, 25th, 75th percentiles and whiskers indicate 1.5 x interquartile range. Black bars indicate means significantly different to day 34 control. Analysed using one-way ANOVA; ASM p=0.035308; ECM p = 0.029165, 0.01833, 0.013959 respectively. **(C)** Area fractions of extra-cellular matrix (ECM; top row) and airway smooth muscle (ASM; bottom row) for all airways from both control and ova-challenged animals at maximal remodelling (day 34) and one week post challenge (day 41). Histograms and corresponding fitted distributions of area fraction of stain at days 34 (left column), and 41 (middle column). All four fitted distributions are shown in the right column (data from 4-6 mice and 90-168 airways for each condition – see **Table 1** for group numbers).

Figure 3: Changes in smooth muscle and extra-cellular matrix stratified by airway size. Airways were categorised as small (basement membrane perimeter < 500μm), medium (500 – 1000μm) and large (1000 – 1500μm); numbers of airways identified in each these groups are given in **Table 2**. Histograms show area fraction of **(A)** extracellular matrix (ECM) and **(B)** airway smooth muscle (ASM) at days 34 (left column), and 41 (middle column). Box plots show change in area fractions of ECM and ASM (right column) on days 34 and 41. Box plots show the median, 25^{th}, 75^{th} percentiles and whiskers the most extreme data points not considered outliers; outliers are highlighted in red. Black bars indicate means are significantly different to mean at day 34 control. Green bars show cases in which there are additional significant differences between means. Analysed using one-way ANOVA; p values shown on figure panels.

Figure 4: Differential changes in airway constituents with airway size under fine stratification. (A) 3D histograms showing frequency of airways (denoted by colour-scale) binned according to both ECM area fraction and size (basement membrane (BM) perimeter). To aid interpretation, 2D projections (top-down views of the 3D histograms in **(A)**, in which colours indicate frequency of observation as

indicated by the colour-bars) are shown instead for **(B)** Extracellular matrix (ECM) and **(C)** airway smooth muscle (ASM) for day 34 control (left column) and day 34 ovalbumin challenged (OVA, right column). Solid white lines indicate lines of "best fit". Dashed white lines are lines of best fit from control data overlaid on the corresponding ovalbumin data for comparison. Interpretation of these, and data for all days, are given in **Supplementary Fig. 4.**

Figure 5: Spatial distribution of smooth muscle and extra-cellular matrix across the airway wall. Area fraction of **(A)** extra-cellular matrix (ECM) and **(B)** airway smooth muscle (ASM) distributed spatially across the airway wall for all control and ovalbumin-challenged (Ova) mice at days 34 and 41. The region between the basement membrane and the outer airway margin defined by the software is scaled from zero (basement membrane side) to one (outer airway margin). Gray curves represent individual airways, and coloured curves indicate average area fraction as function of normalized airway radius and shown in summary in **(C)**. The yellow shaded region indicates increased ECM between control D34 and control D41 (not significant). Purple shaded region shows increase in ECM content between control D41 and ova D41 (not significant). Distributions for individual mice are given in **Supplementary Fig. 3.**

Figure 6: Changes in normalized epithelial area (A) Changes in epithelial area at days 34 and 41. Epithelial area normalized with respect to basement membrane (BM) perimeter for all airways from both control and ovalbumin-challenged (ova) animals. Histograms and corresponding fitted distributions of epithelial area at days 34 and 41. **(B)** Global changes in epithelial area during resolution period. Box plots showing change in epithelial area from days 34 to 41. Box plots show the median, 25^{th}, 75^{th} percentiles and whiskers the most extreme data points not considered outliers; outliers are highlighted in red. Black bars indicate means that are significantly different to mean at day 34 control (p values indicated in text; 4-6 mice and 90-186 airways per group - see **Table 1** (αSMA) for group numbers). **(C)** Changes in epithelial area graded by airway size. Airways were categorised as small (BM

perimeter < 500μm), medium (500 – 1000μm), and large (1000 – 1500μm). Histograms show epithelial area at days 34 and 41 (see **Table 2** (αSMA) for group numbers). **(D)** Summary data box plots showing change in epithelial area on days 34 and 41 corresponding to the airway size. Black bars indicate means are significantly different to control at day 34. Green bars show additional significant differences between means. **(E)** Differential changes in epithelial area with airway size under finer stratification. 2D projections of 3D histograms showing frequency of airways (denoted by colour-scale) binned according to both epithelial area and size (basement membrane perimeter) at day 34. White lines indicate lines of "best fit". Interpretation of these is given in **Supplementary Fig. 4**.

Figure 7: Airway-area relationships explained by simulated data. Inner, lumen and epithelial areas are computed as described in **Supplementary Figure 5**. Simulated lumen and inner area OVA data is obtained by perturbing control data at day 34 by a normally-distributed random amount (see Supplement). Panels show area distributions normalised with respect to the BM perimeter for control and OVA data and simulated OVA data at day 34 (left), and corresponding box plots (right). Box plots show the median, 25^{th}, 75^{th} percentiles and whiskers the most extreme data points not considered outliers; outliers are highlighted in red. (A) Inner area normalised with respect to the BM perimeter is significantly increased in ova compared with control at day 34, indicated by the shift in the peak in the distributions (left) as well as one-way ANOVA and box plots (right). (B) Lumen area is not significantly different. (C) Mean epithelial area is significantly increased. Analysed using using one-way ANOVA; p values given in text.

References

1. Krings JG, Goss CW, Lew D, Samant M, McGregor MC, Boomer J, et al. Quantitative CT metrics are associated with longitudinal lung function decline and future asthma exacerbations: Results from SARP-3. *The Journal of allergy and clinical immunology.* 2021.
2. Patyk M, Obojski A, Sokolowska-Dabek D, Parkitna-Patyk M, and Zaleska-Dorobisz U. Airway wall thickness and airflow limitations in asthma assessed in quantitative computed tomography. *Ther Adv Respir Dis.* 2020;14:1753466619898598.
3. Kim S, Lee CH, Jin KN, Cho SH, and Kang HR. Severe Asthma Phenotypes Classified by Site of Airway Involvement and Remodeling via Chest CT Scan. *J Investig Allergol Clin Immunol.* 2018;28(5):312-20.
4. Jiang D, Wang Z, Yu N, Shen C, Deng L, and Guo Y. Airway Remodeling in Asthma: Evaluation in 5 Consecutive Bronchial Generations by Using High-Resolution Computed Tomography. *Respir Care.* 2018;63(11):1399-406.
5. James AL, and Wenzel S. Clinical relevance of airway remodelling in airway diseases. *Eur Respir J.* 2007;30(1):134-55.
6. Aun MV, Bonamichi-Santos R, Arantes-Costa FM, Kalil J, and Giavina-Bianchi P. Animal models of asthma: utility and limitations. *J Asthma Allergy.* 2017;10:293-301.
7. Donovan GM, and Noble PB. Small airways vs large airways in asthma: time for a new perspective. *J Appl Physiol (1985).* 2021.
8. Locke NR, Royce SG, Wainewright JS, Samuel CS, and Tang ML. Comparison of airway remodeling in acute, subacute, and chronic models of allergic airways disease. *Am J Respir Cell Mol Biol.* 2007;36(5):625-32.
9. Klein M, Vignaud JM, Hennequin V, Toussaint B, Bresler L, Plenat F, et al. Increased expression of the vascular endothelial growth factor is a pejorative prognosis marker in papillary thyroid carcinoma. *J Clin Endocr Metab.* 2001;86(2):656-8.
10. Parkin E, O'Reilly DA, Plumb AA, Manoharan P, Rao M, Coe P, et al. Digital histology quantification of intra-hepatic fat in patients undergoing liver resection. *European Journal of Surgical Oncology.*41(8):1020-7.
11. Schneider CA, Rasband WS, and Eliceiri KW. NIH Image to ImageJ: 25 years of image analysis. *Nat Methods.* 2012;9(7):671-5.
12. Schindelin J, Arganda-Carreras I, Frise E, Kaynig V, Longair M, Pietzsch T, et al. Fiji: an open-source platform for biological-image analysis. *Nat Methods.* 2012;9(7):676-82.
13. Tatler AL, John AE, Jolly L, Habgood A, Porte J, Brightling C, et al. Integrin alphavbeta5-mediated TGF-beta activation by airway smooth muscle cells in asthma. *J Immunol.* 2011;187(11):6094-107.
14. Cairns JT, Habgood A, Edwards-Pritchard RC, Joseph C, John AE, Wilkinson C, et al. Loss of ELK1 has differential effects on age-dependent organ fibrosis. *Int J Biochem Cell Biol.* 2020;120:105668.
15. Soutiere SE, Tankersley CG, and Mitzner W. Differences in alveolar size in inbred mouse strains. *Respiratory physiology & neurobiology.* 2004;140(3):283-91.
16. Thiesse J, Namati E, Sieren JC, Smith AR, Reinhardt JM, Hoffman EA, et al. Lung structure phenotype variation in inbred mouse strains revealed through in vivo micro-CT imaging. *J Appl Physiol (1985).* 2010;109(6):1960-8.
17. Discher DE, Mooney DJ, and Zandstra PW. Growth factors, matrices, and forces combine and control stem cells. *Science (New York, NY.* 2009;324(5935):1673-7.
18. Humphrey JD, Dufresne ER, and Schwartz MA. Mechanotransduction and extracellular matrix homeostasis. *Nat Rev Mol Cell Biol.* 2014;15(12):802-12.
19. Swartz MA, Tschumperlin DJ, Kamm RD, and Drazen JM. Mechanical stress is communicated between different cell types to elicit matrix remodeling. *Proceedings of the National Academy of Sciences of the United States of America.* 2001;98(11):6180-5.

20. Tschumperlin DJ, and Drazen JM. Mechanical stimuli to airway remodeling. *American journal of respiratory and critical care medicine.* 2001;164(10 Pt 2):S90-4.
21. Maghsoudi-Ganjeh M, Sattari S, and Eskandari M. Mechanical behavior of the airway wall in respiratory disease. *Curr Opin Physiol.* 2021;22.
22. Pascoe CD, Seow CY, Hackett TL, Pare PD, and Donovan GM. Heterogeneity of airway wall dimensions in humans: a critical determinant of lung function in asthmatics and nonasthmatics. *American journal of physiology.* 2017;312(3):L425-L31.
23. Lutchen KR. Invited Editorial on "Measurement of intraindividual airway tone heterogeneity and its importance in asthma": How does an airway and subsequently the lung become hyperresponsive? *J Appl Physiol (1985).* 2016;121(1):221-2.
24. Carroll N, Elliot J, Morton A, and James A. The structure of large and small airways in nonfatal and fatal asthma. *The American review of respiratory disease.* 1993;147(2):405-10.
25. James A, Mauad T, Abramson M, and Green F. Airway smooth muscle hypertrophy and hyperplasia in asthma. *American journal of respiratory and critical care medicine.* 2012;186(6):568; author reply 9.
26. Brown RH, Pearse DB, Pyrgos G, Liu MC, Togias A, and Permutt S. The structural basis of airways hyperresponsiveness in asthma. *J Appl Physiol (1985).* 2006;101(1):30-9.
27. Brown RH, and Togias A. Measurement of intraindividual airway tone heterogeneity and its importance in asthma. *J Appl Physiol (1985).* 2016;121(1):223-32.
28. Ma X, Li W, and Stephens NL. Heterogeneity of airway smooth muscle at tissue and cellular levels. *Can J Physiol Pharmacol.* 1997;75(7):930-5.
29. Kaczka DW, Massa CB, and Simon BA. Reliability of estimating stochastic lung tissue heterogeneity from pulmonary impedance spectra: a forward-inverse modeling study. *Annals of biomedical engineering.* 2007;35(10):1722-38.
30. Eskandari M, Arvayo AL, and Levenston ME. Mechanical properties of the airway tree: heterogeneous and anisotropic pseudoelastic and viscoelastic tissue responses. *J Appl Physiol (1985).* 2018;125(3):878-88.
31. Takizawa H. Remodeling in small airways of asthma. *Respiratory Medicine CME.* 2008;1(2):69-74.
32. James AL, Donovan GM, Green FHY, Mauad T, Abramson MJ, Cairncross A, et al. Heterogeneity of Airway Smooth Muscle Remodelling in Asthma. *Am J Respir Crit Care Med.* 2022.
33. Wagers S, Lundblad LK, Ekman M, Irvin CG, and Bates JH. The allergic mouse model of asthma: normal smooth muscle in an abnormal lung? *J Appl Physiol (1985).* 2004;96(6):2019-27.
34. Lilburn DM, Tatler AL, Six JS, Lesbats C, Habgood A, Porte J, et al. Investigating lung responses with functional hyperpolarized xenon-129 MRI in an ex vivo rat model of asthma. *Magn Reson Med.* 2016;76(4):1224-35.
35. Yanai M, Sekizawa K, Ohrui T, Sasaki H, and Takishima T. Site of airway obstruction in pulmonary disease: direct measurement of intrabronchial pressure. *J Appl Physiol (1985).* 1992;72(3):1016-23.
36. Hirota JA, Ellis R, and Inman MD. Regional differences in the pattern of airway remodeling following chronic allergen exposure in mice. *Respiratory research.* 2006;7:120.
37. Kuwano K, Bosken CH, Pare PD, Bai TR, Wiggs BR, and Hogg JC. Small airways dimensions in asthma and in chronic obstructive pulmonary disease. *The American review of respiratory disease.* 1993;148(5):1220-5.
38. Saetta M, Di Stefano A, Rosina C, Thiene G, and Fabbri LM. Quantitative structural analysis of peripheral airways and arteries in sudden fatal asthma. *The American review of respiratory disease.* 1991;143(1):138-43.
39. Bergeron C, Hauber HP, Gotfried M, Newman K, Dhanda R, Servi RJ, et al. Evidence of remodeling in peripheral airways of patients with mild to moderate asthma: effect of hydrofluoroalkane-flunisolide. *The Journal of allergy and clinical immunology.* 2005;116(5):983-9.

40. Donovan C, Royce SG, Esposito J, Tran J, Ibrahim ZA, Tang ML, et al. Differential effects of allergen challenge on large and small airway reactivity in mice. *PLoS One.* 2013;8(9):e74101.
41. Dolhnikoff M, da Silva LF, de Araujo BB, Gomes HA, Fernezlian S, Mulder A, et al. The outer wall of small airways is a major site of remodeling in fatal asthma. *The Journal of allergy and clinical immunology.* 2009;123(5):1090-7, 7 e1.
42. Southam DS, Ellis R, Wattie J, and Inman MD. Components of airway hyperresponsiveness and their associations with inflammation and remodeling in mice. *The Journal of allergy and clinical immunology.* 2007;119(4):848-54.
43. Ramos-Barbon D, Presley JF, Hamid QA, Fixman ED, and Martin JG. Antigen-specific CD4+ T cells drive airway smooth muscle remodeling in experimental asthma. *The Journal of clinical investigation.* 2005;115(6):1580-9.
44. Alrifai M, Marsh LM, Dicke T, Kilic A, Conrad ML, Renz H, et al. Compartmental and temporal dynamics of chronic inflammation and airway remodelling in a chronic asthma mouse model. *PLoS One.* 2014;9(1):e85839.
45. Yaziji H, and Barry T. Diagnostic Immunohistochemistry: what can go wrong? *Adv Anat Pathol.* 2006;13(5):238-46.

A

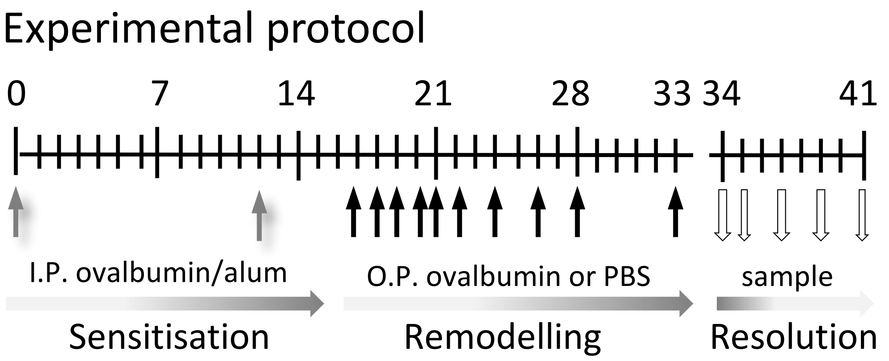

B

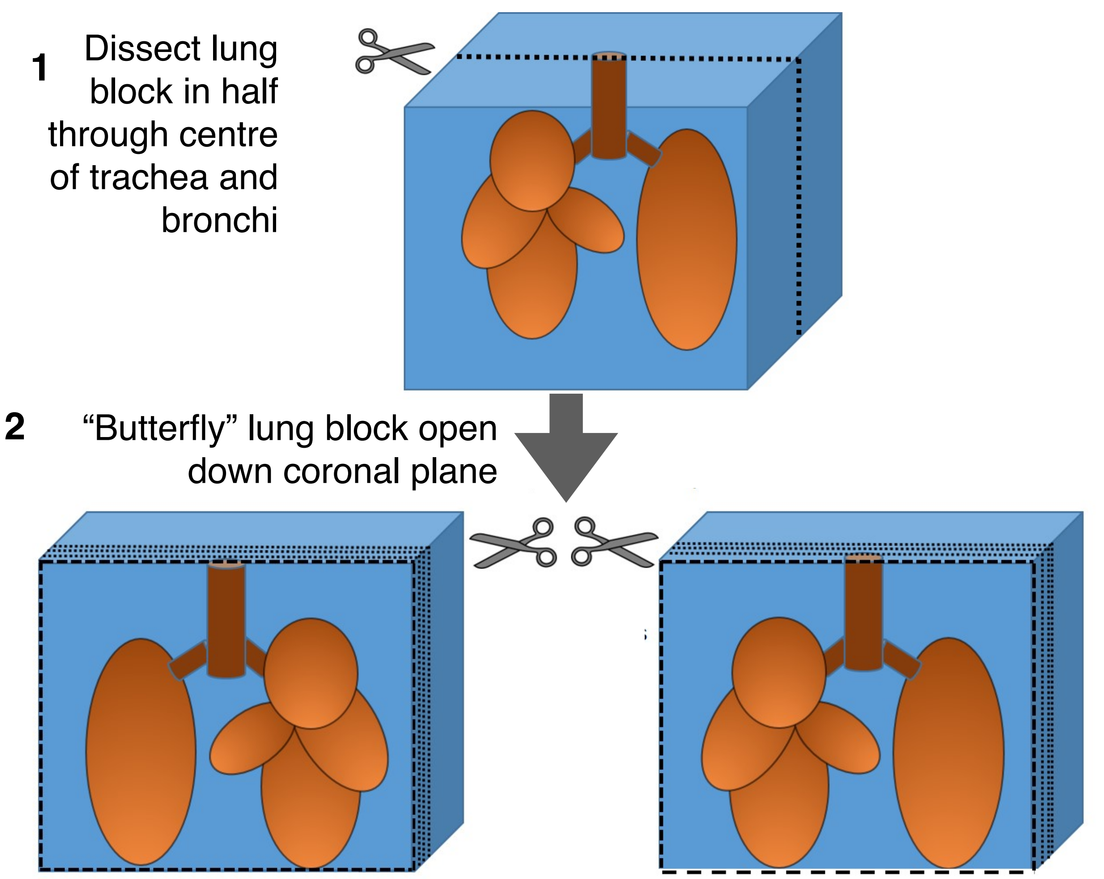

C

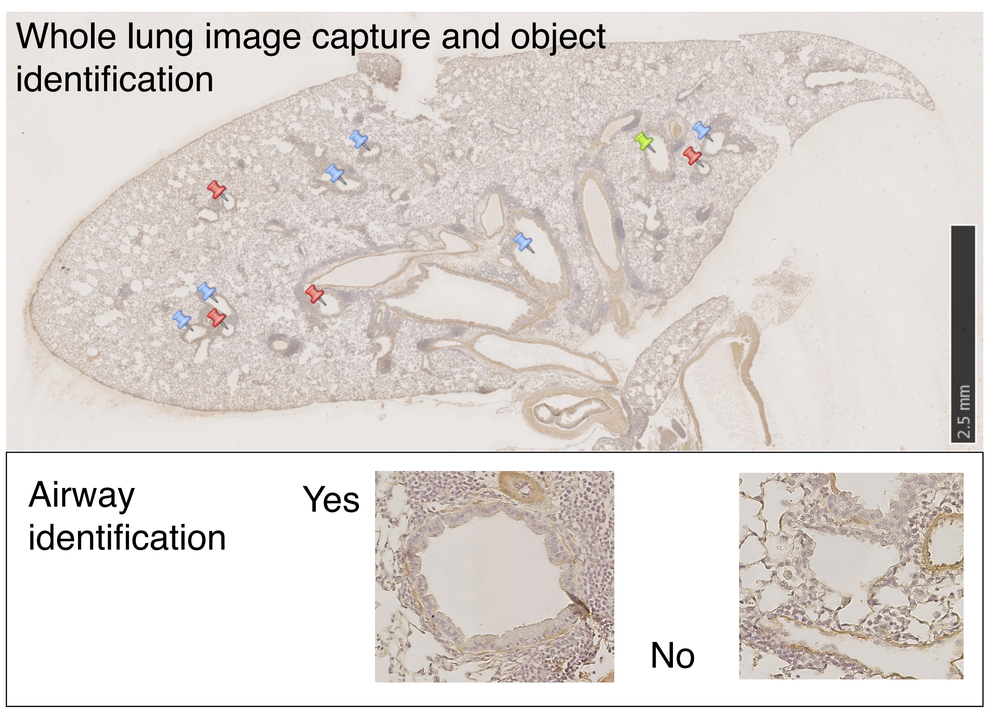

D

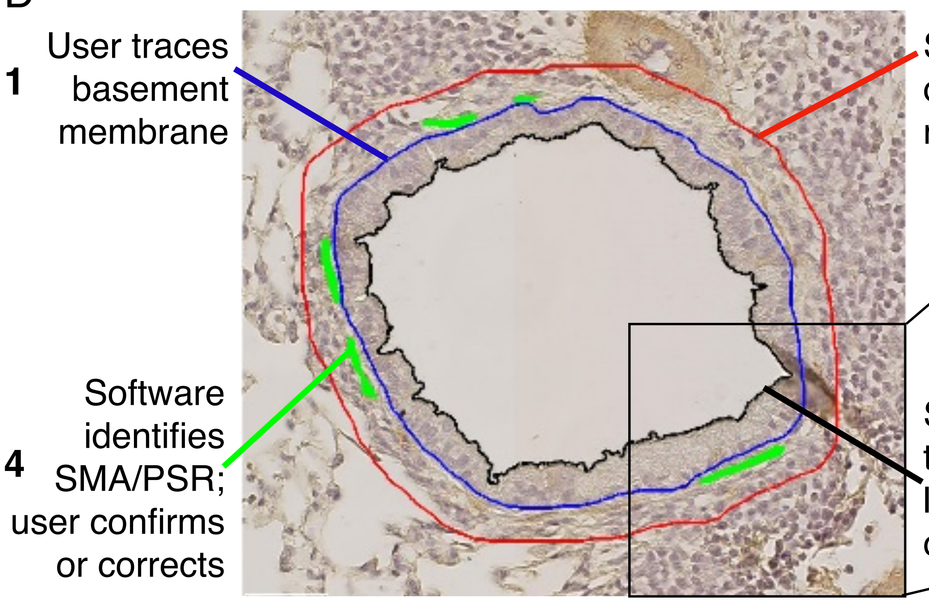

E

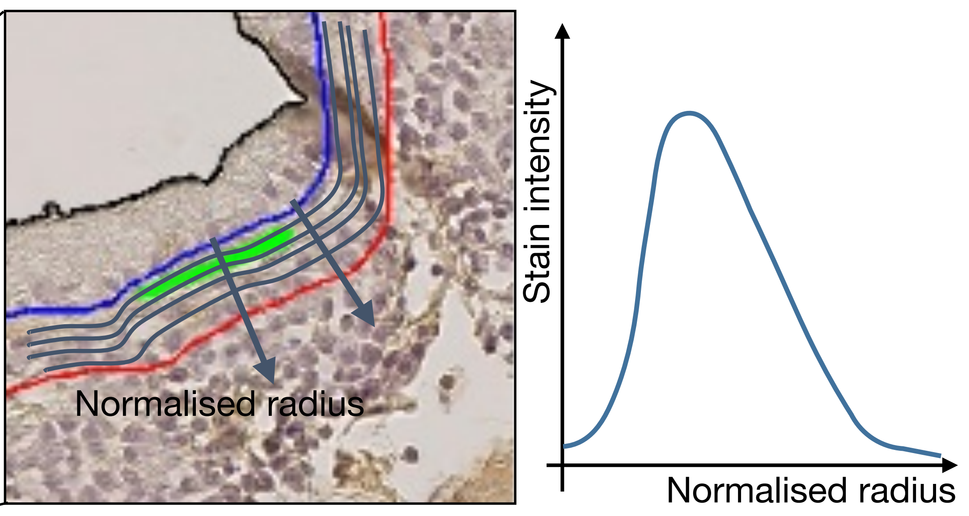

A

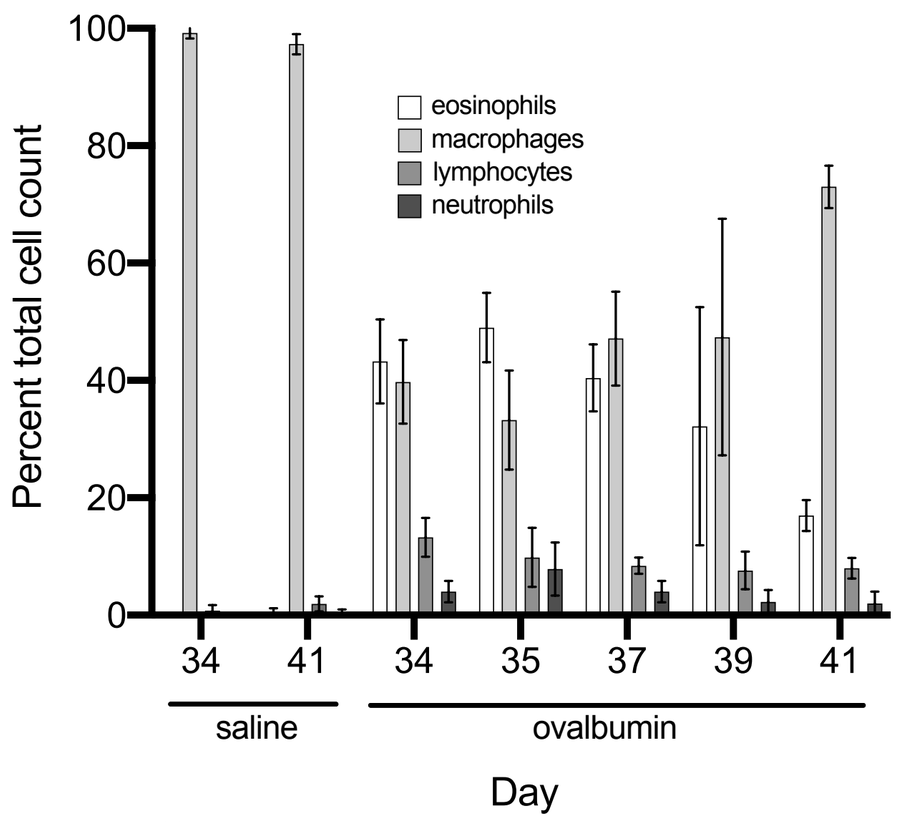

B

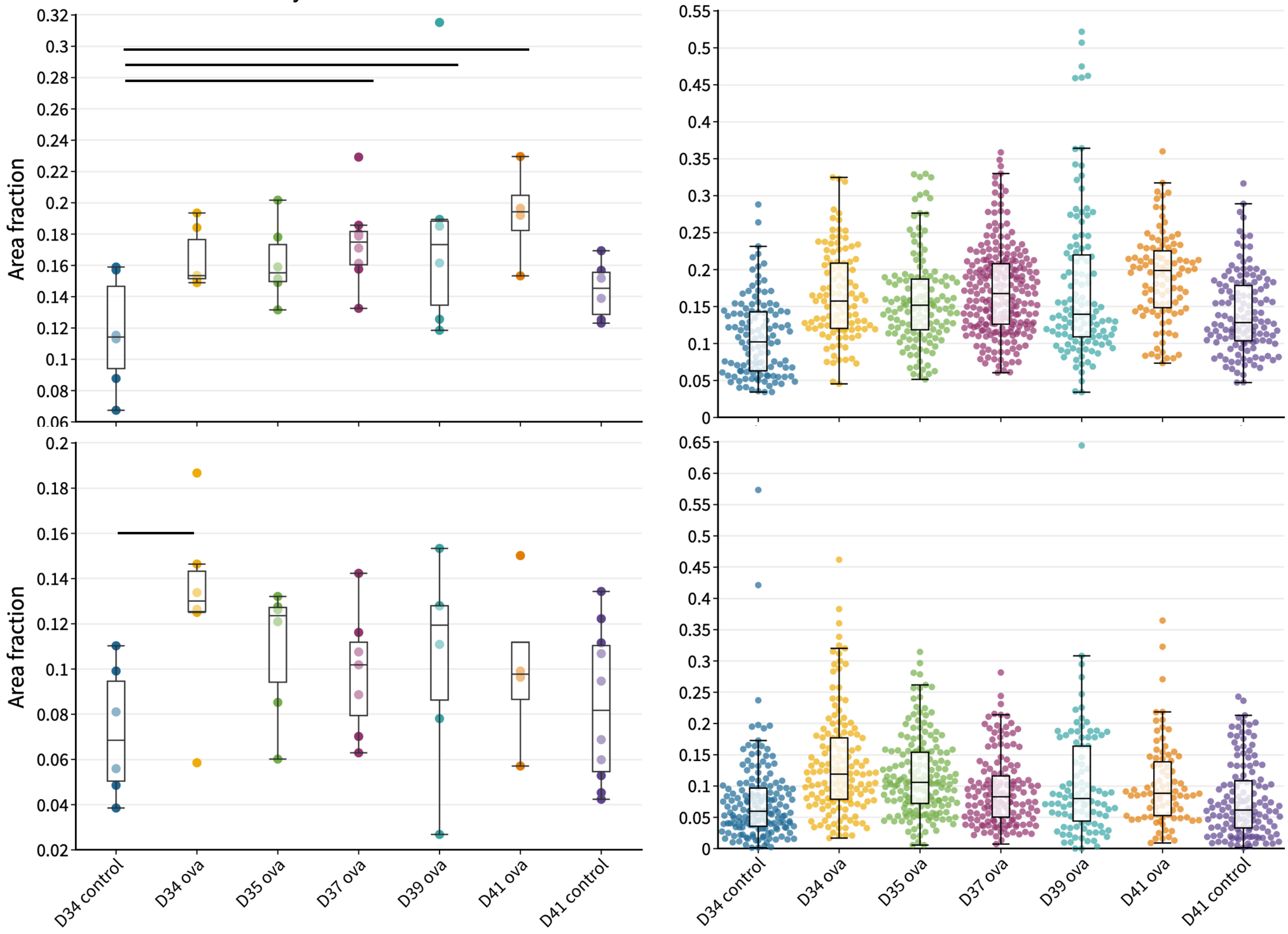

C

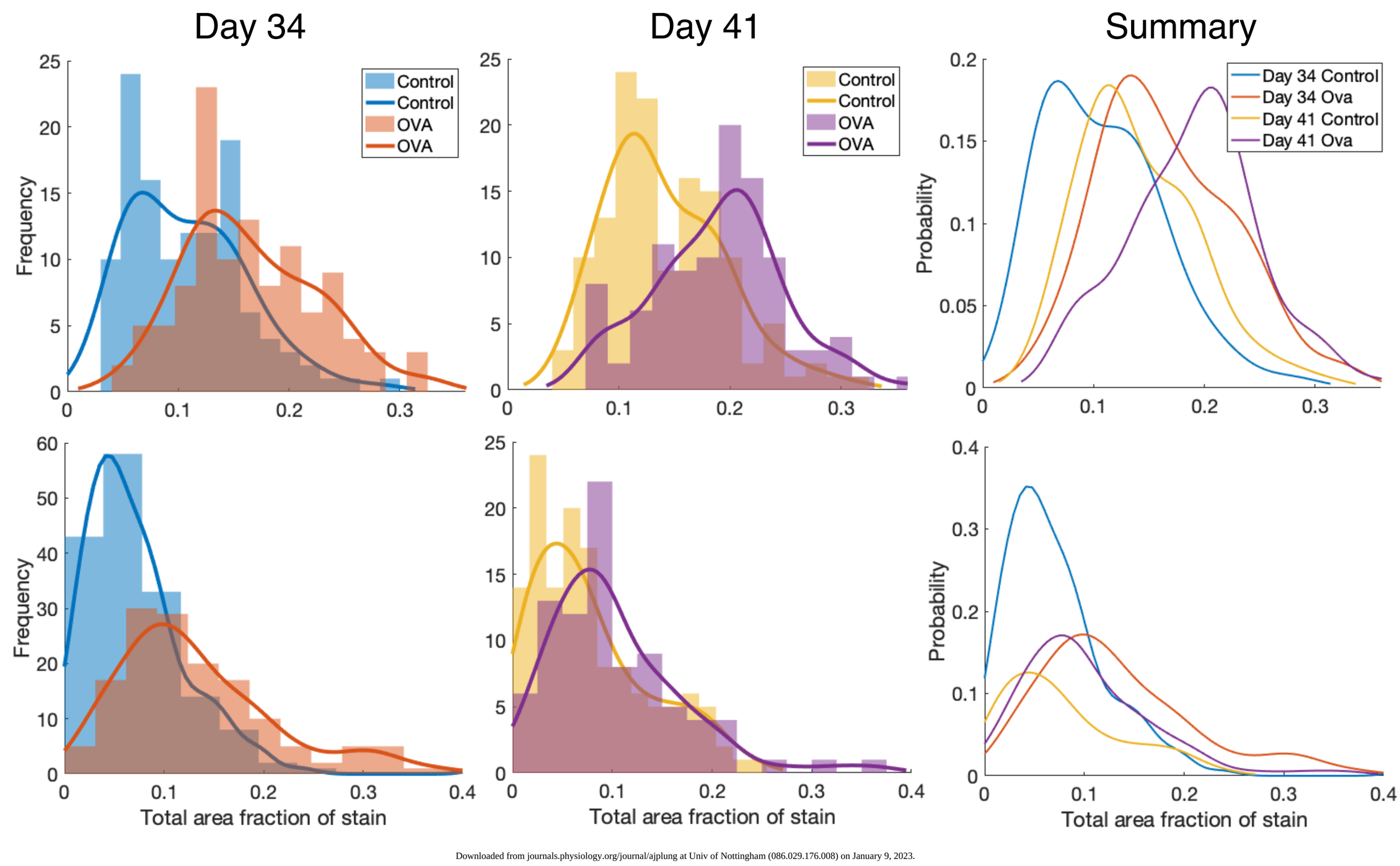

A. ECM

Day 34

Day 41

Summary

Small

Medium

Large

Control

Ova

Frequency

Total area fraction of stain

p=2e-4

p=1e-9

p=2.6e-3

D34 control

D34 ova

D41 control

D41 ova

B. ASM

Day 34

Day 41

Summary

Small

Medium

Large

Control

OVA

Frequency

Total area fraction of stain

p=2.3e-3

p=1.3e-7

p=2.9e-3

D34 control

D34 ova

D41 control

D41 ova

A

3D histogram ECM

Day 34 control

Number of airways

Area fraction of stain

BM perimeter [μm]

Day 34 ova

Number of airways

Area fraction of stain

BM perimeter [μ m]

B

ECM

BM perimeter [μm]

C

ASM

BM perimeter [μm]

Area fraction stain

A

Control

Ova

ECM

Day 34

Day 41

B

ASM

Day 34

Day 41

Area faction of stain

Normalised airway radius

C

Summary

ECM

ASM

D34 control

D34 ova

D41 control

D41 ova

Area fraction of stain

Normalised airway radius

A

Day 34

Day 41

B

Summary

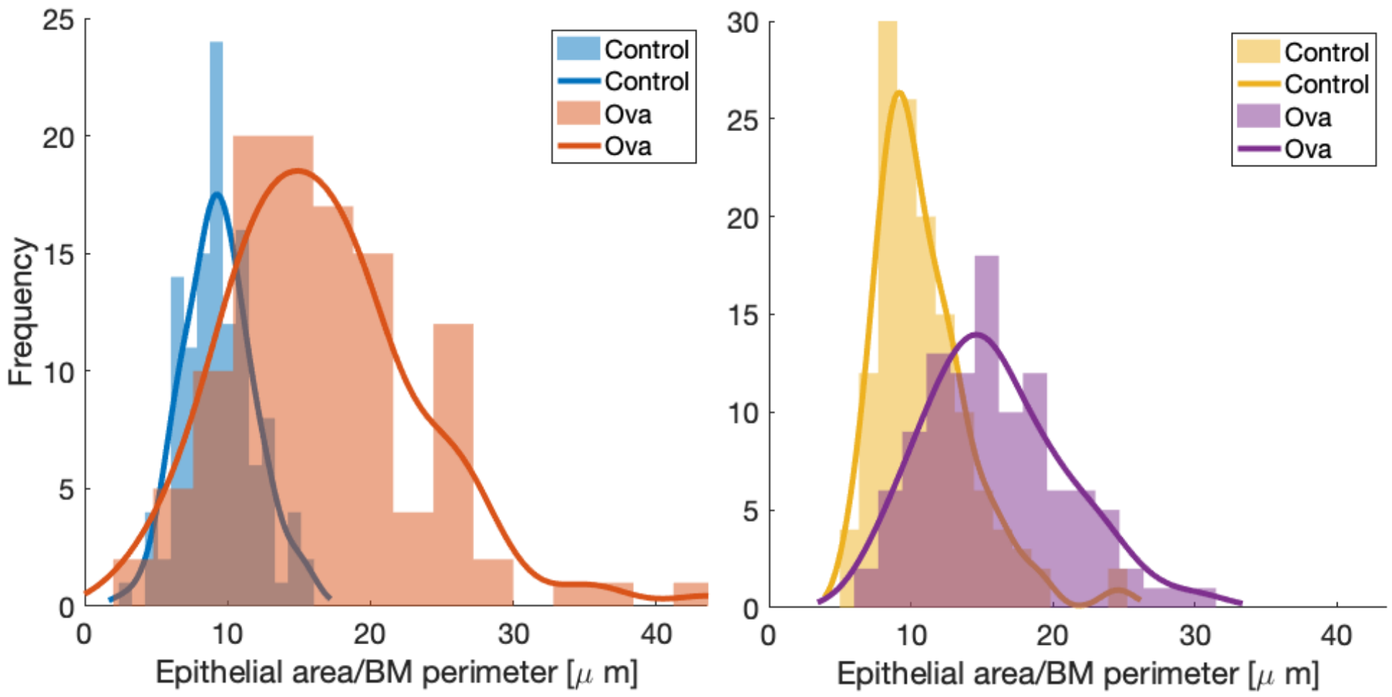

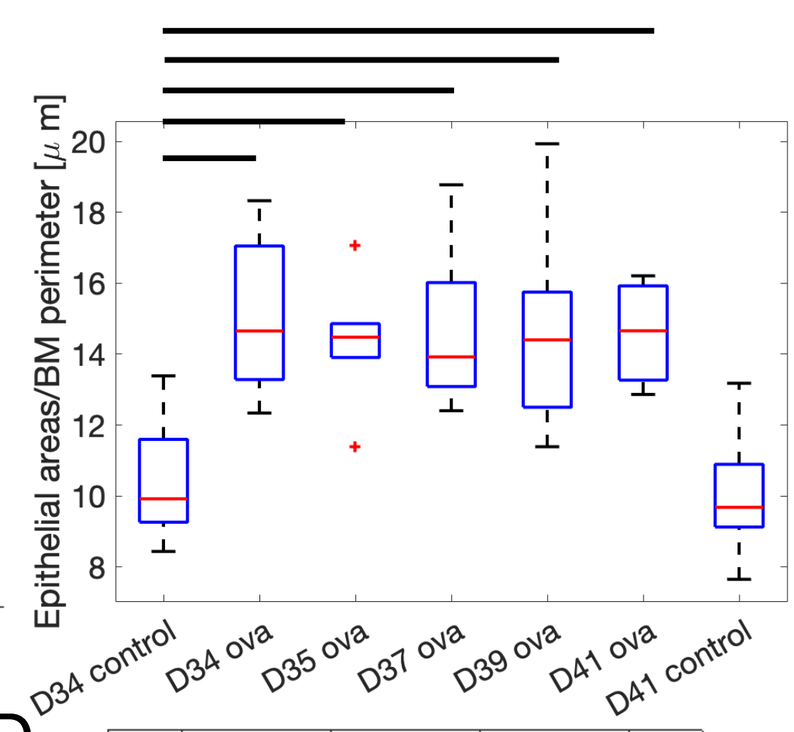

C

Small

Medium

Large

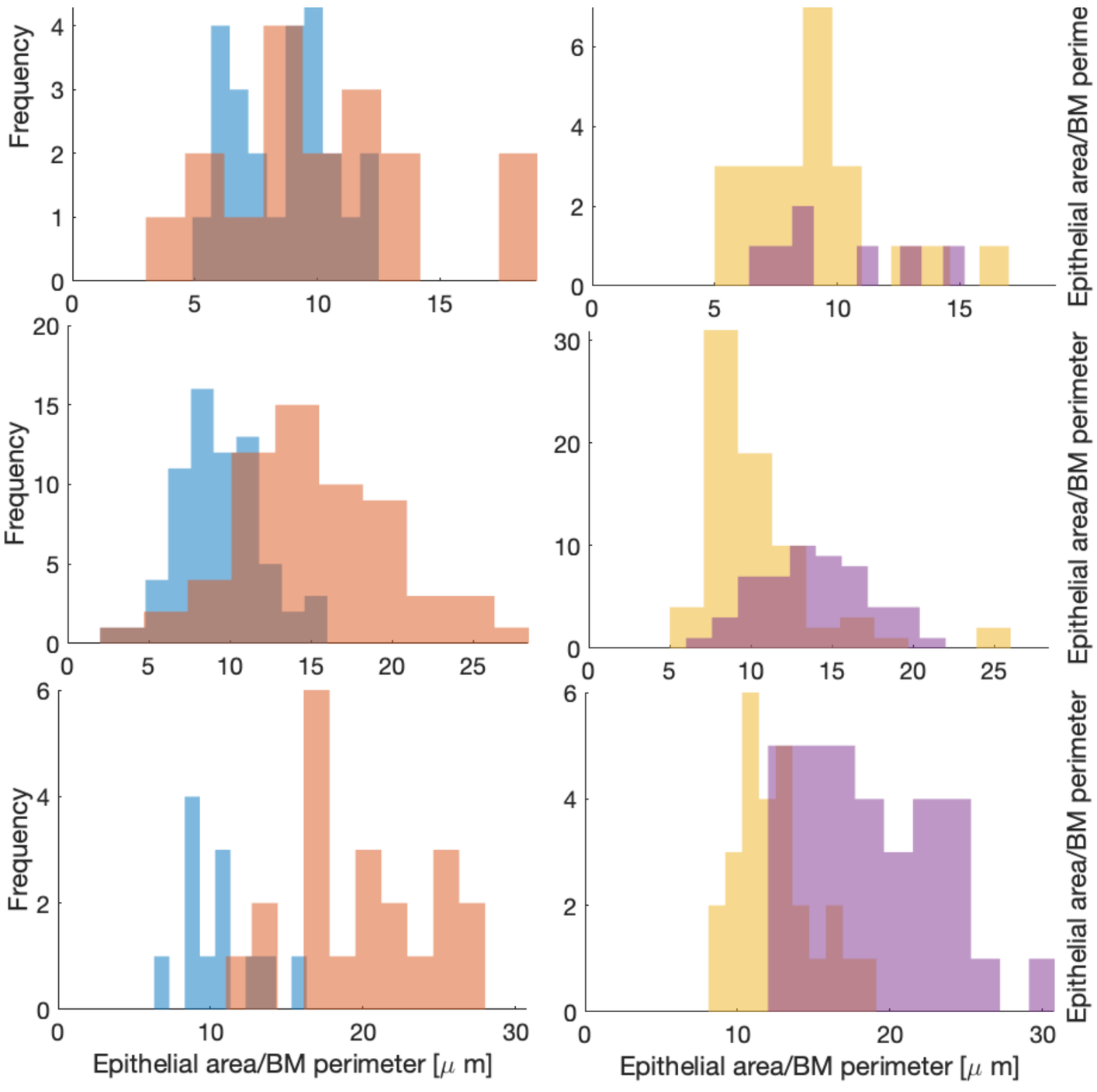

D

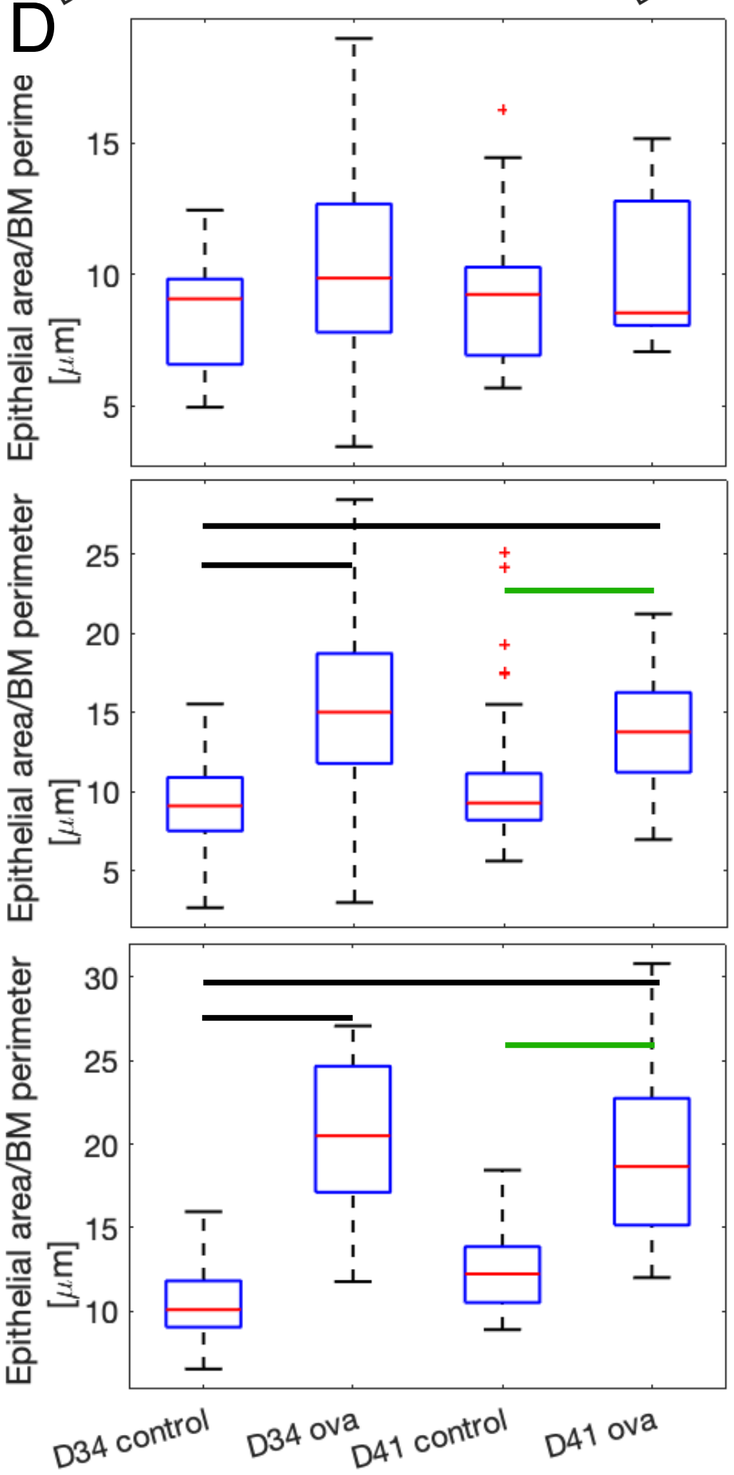

E

Day 34 control

Day 34 ova

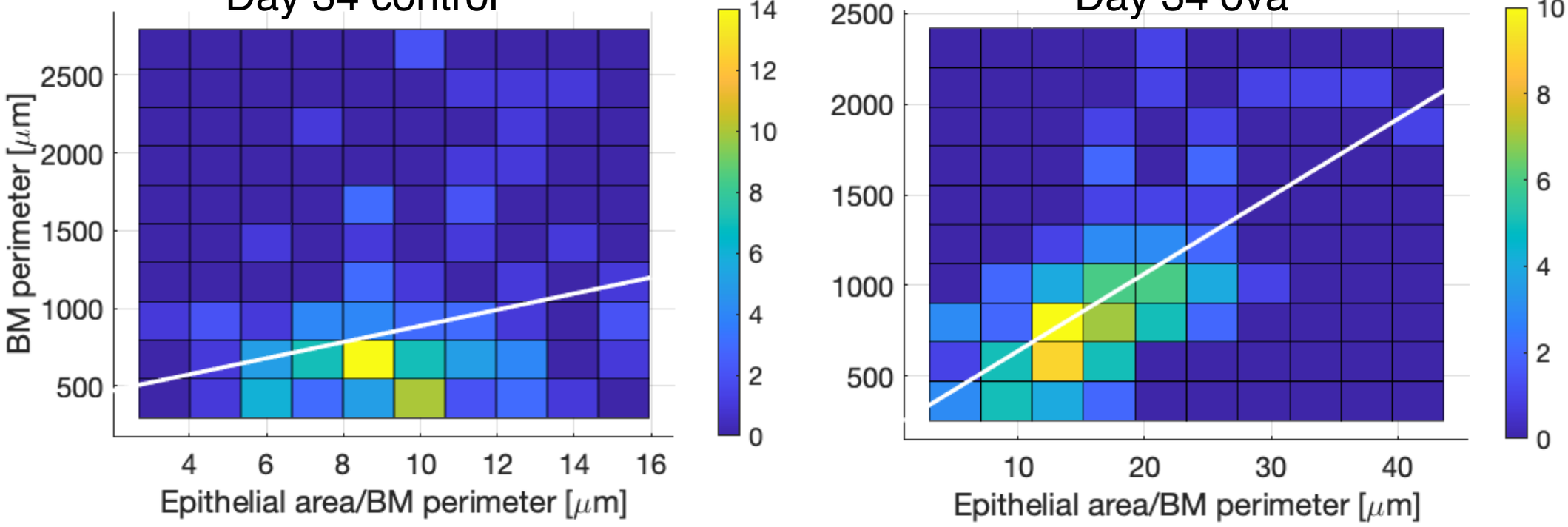

A

Inner area

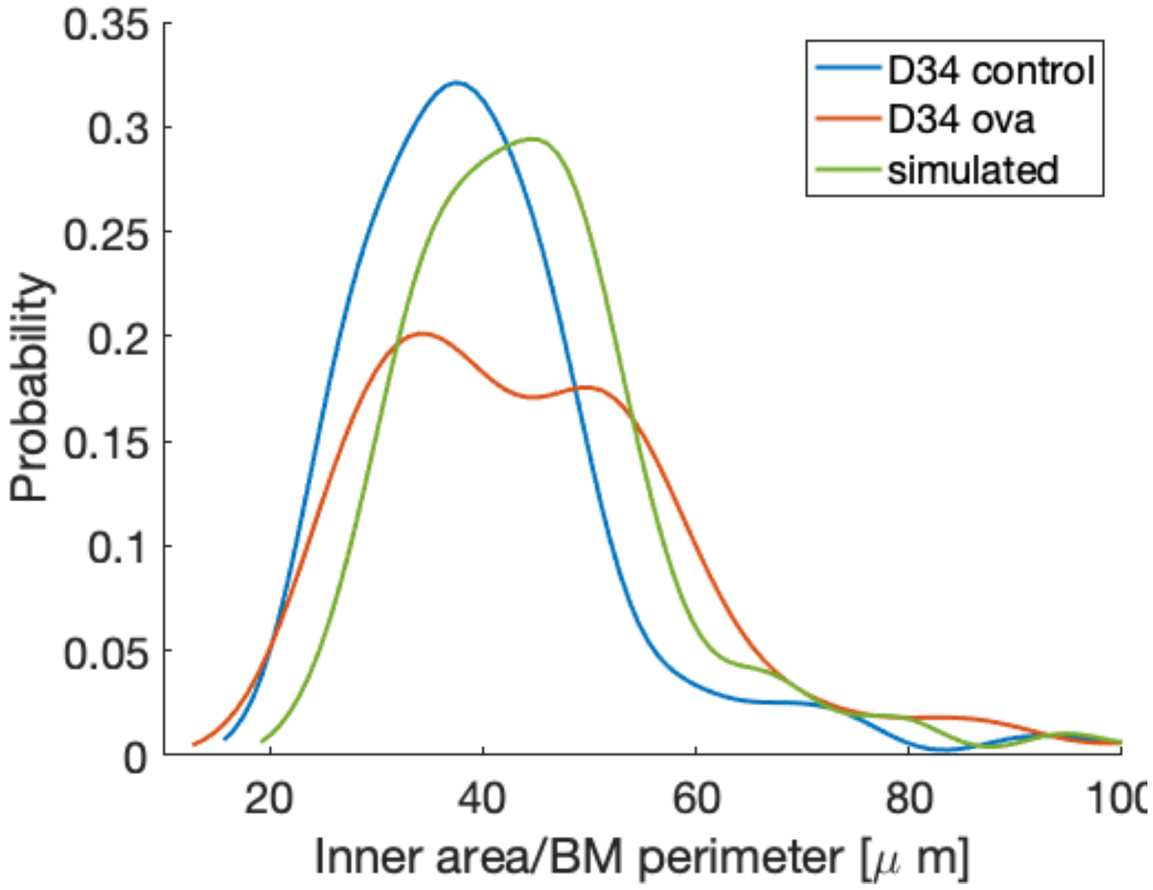

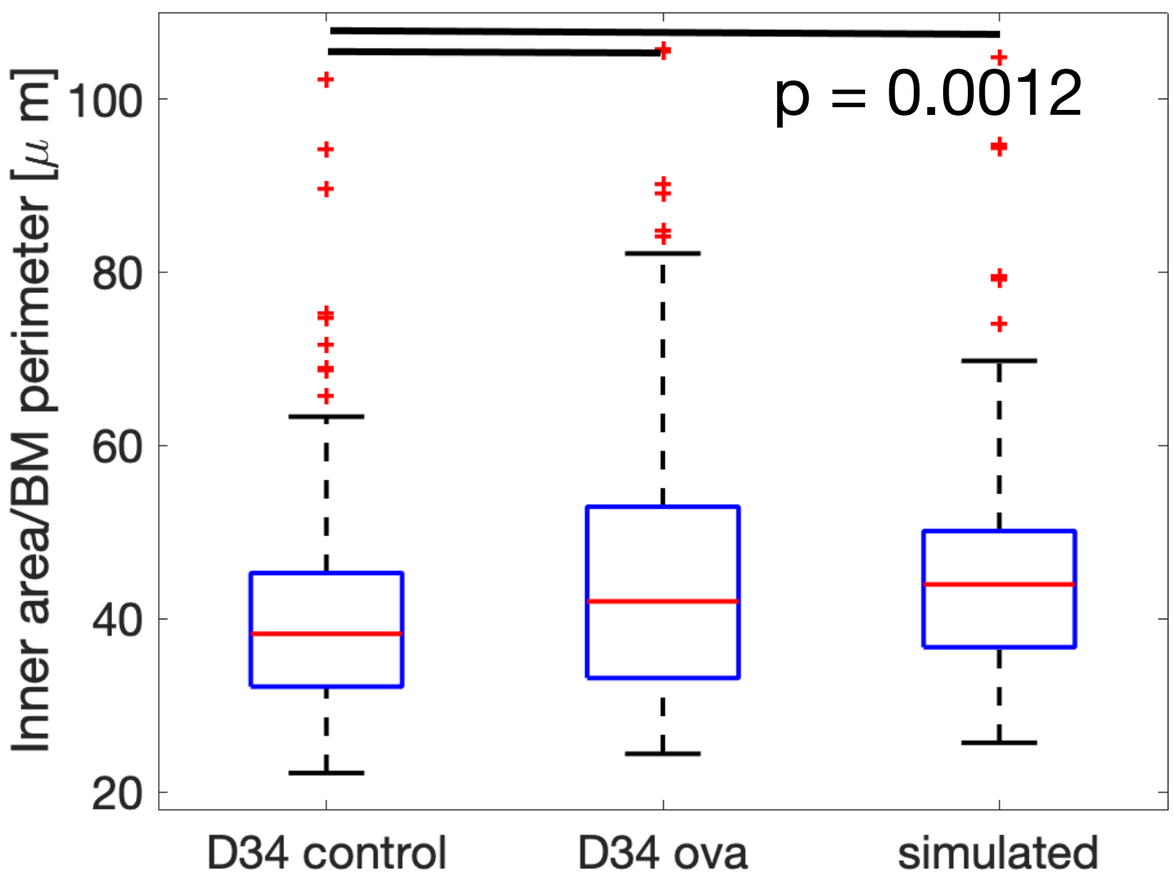

B

Lumen area

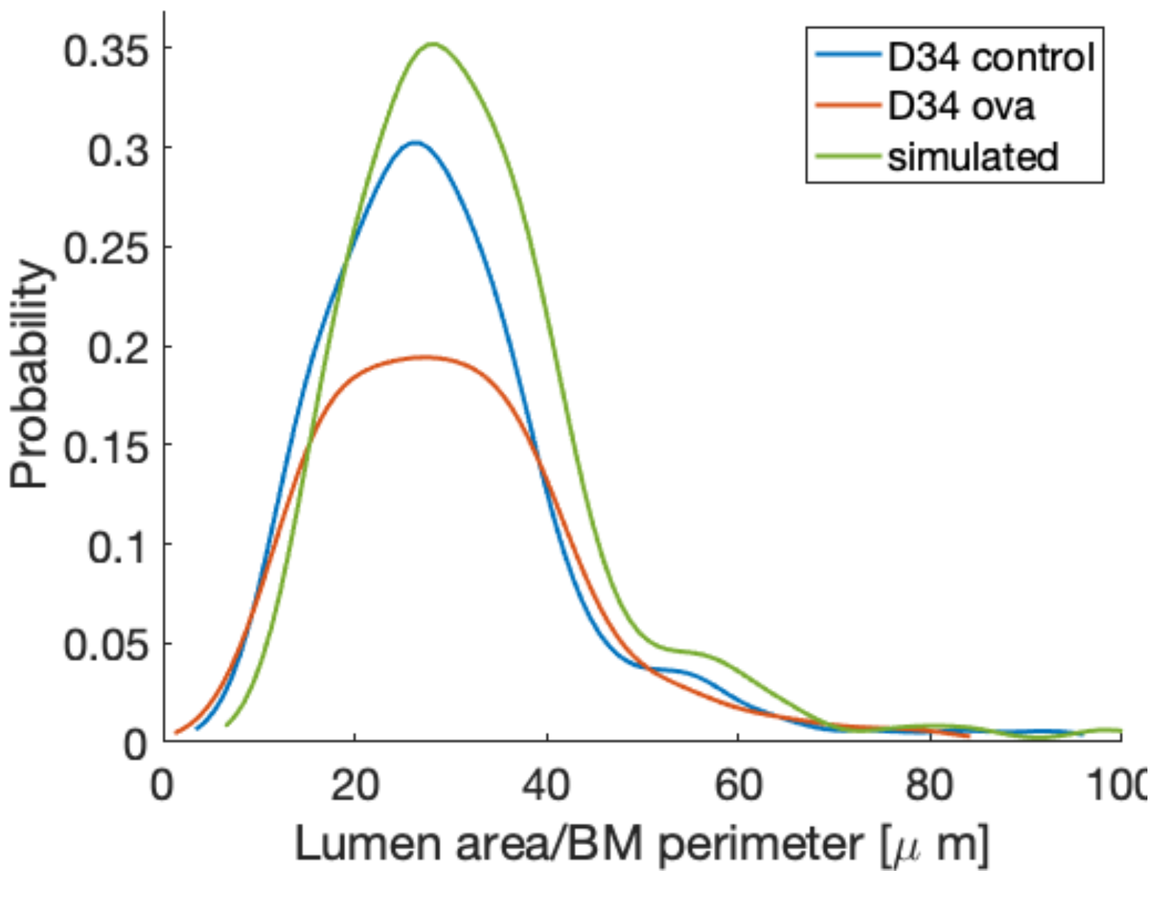

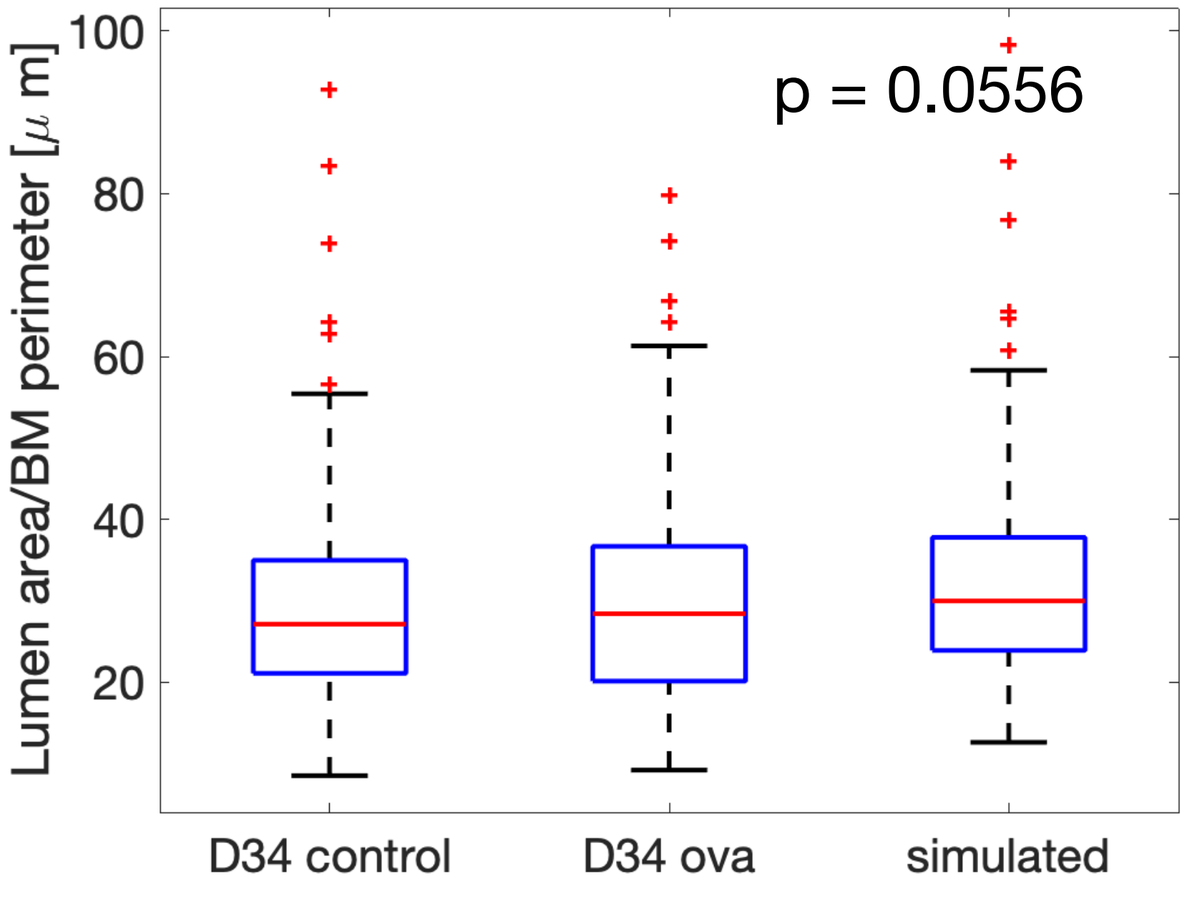

C

Epithelial area

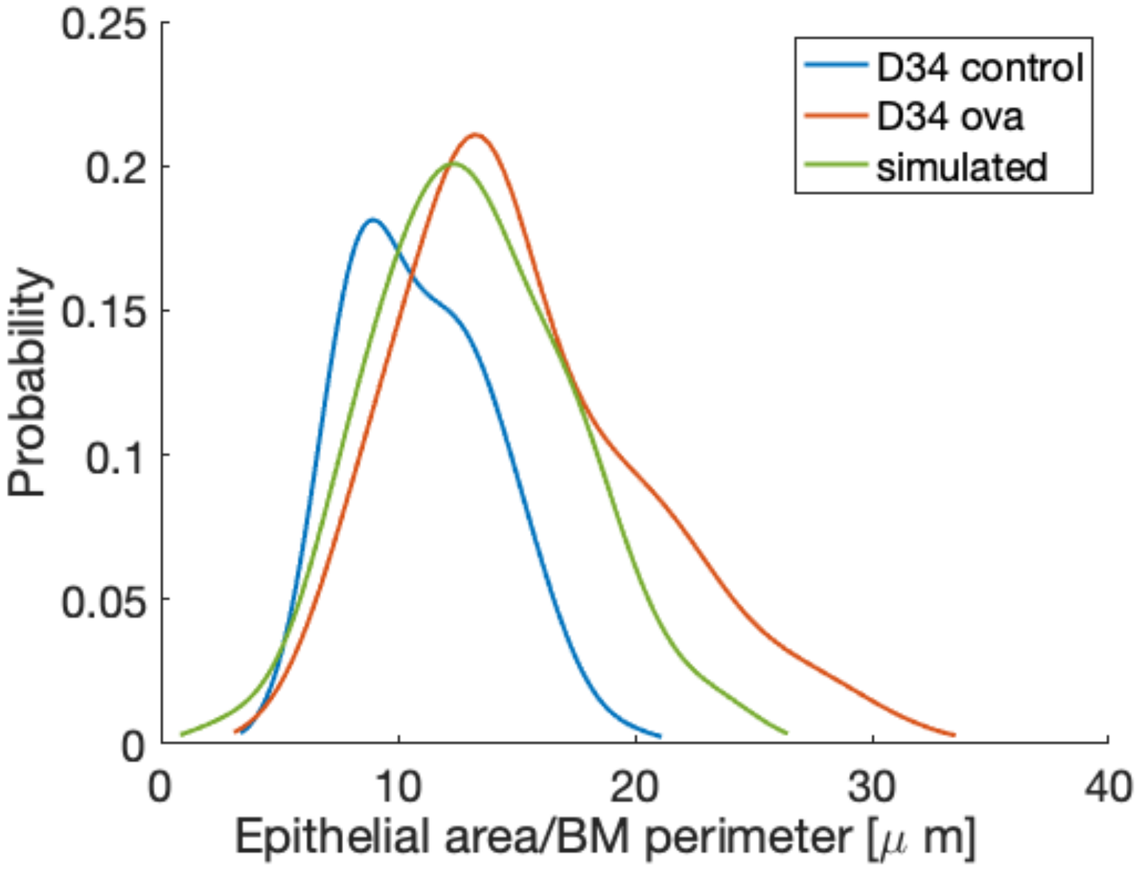

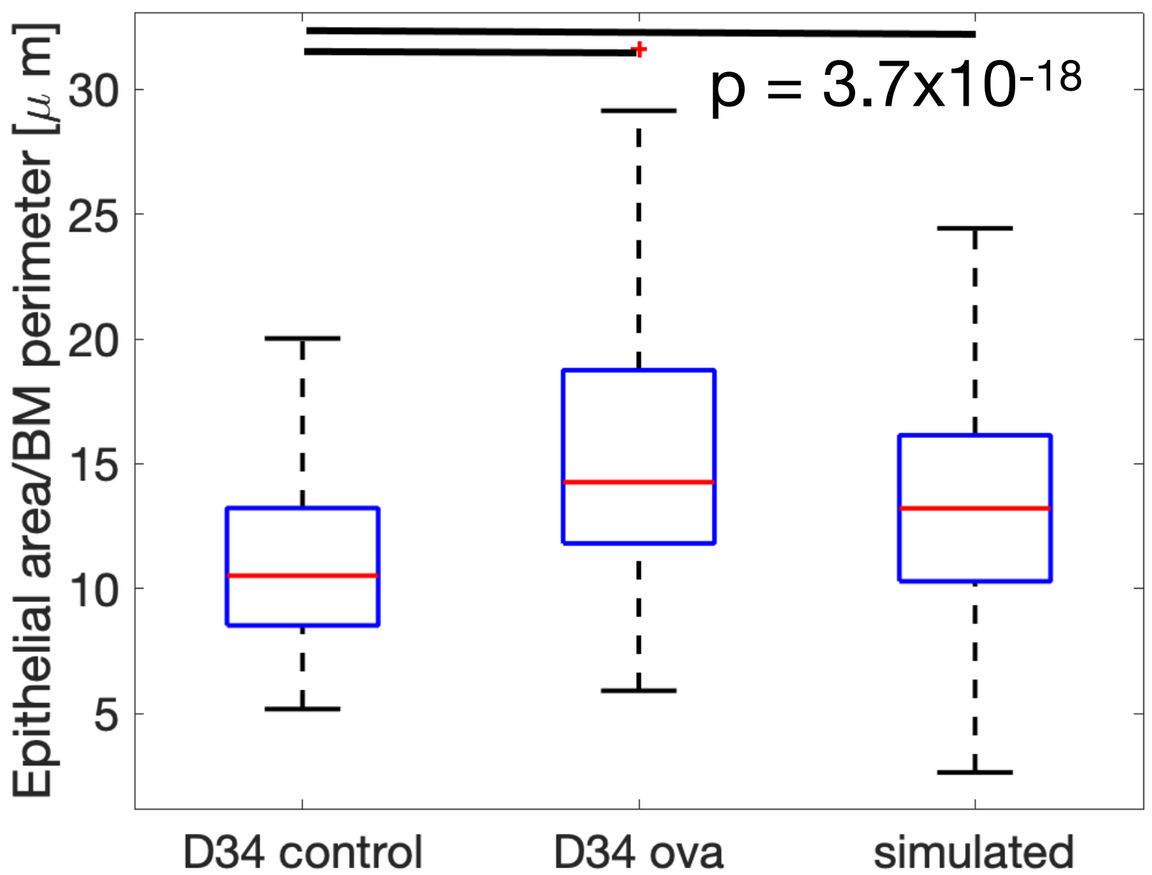

Differential remodelling in a mouse model of asthma

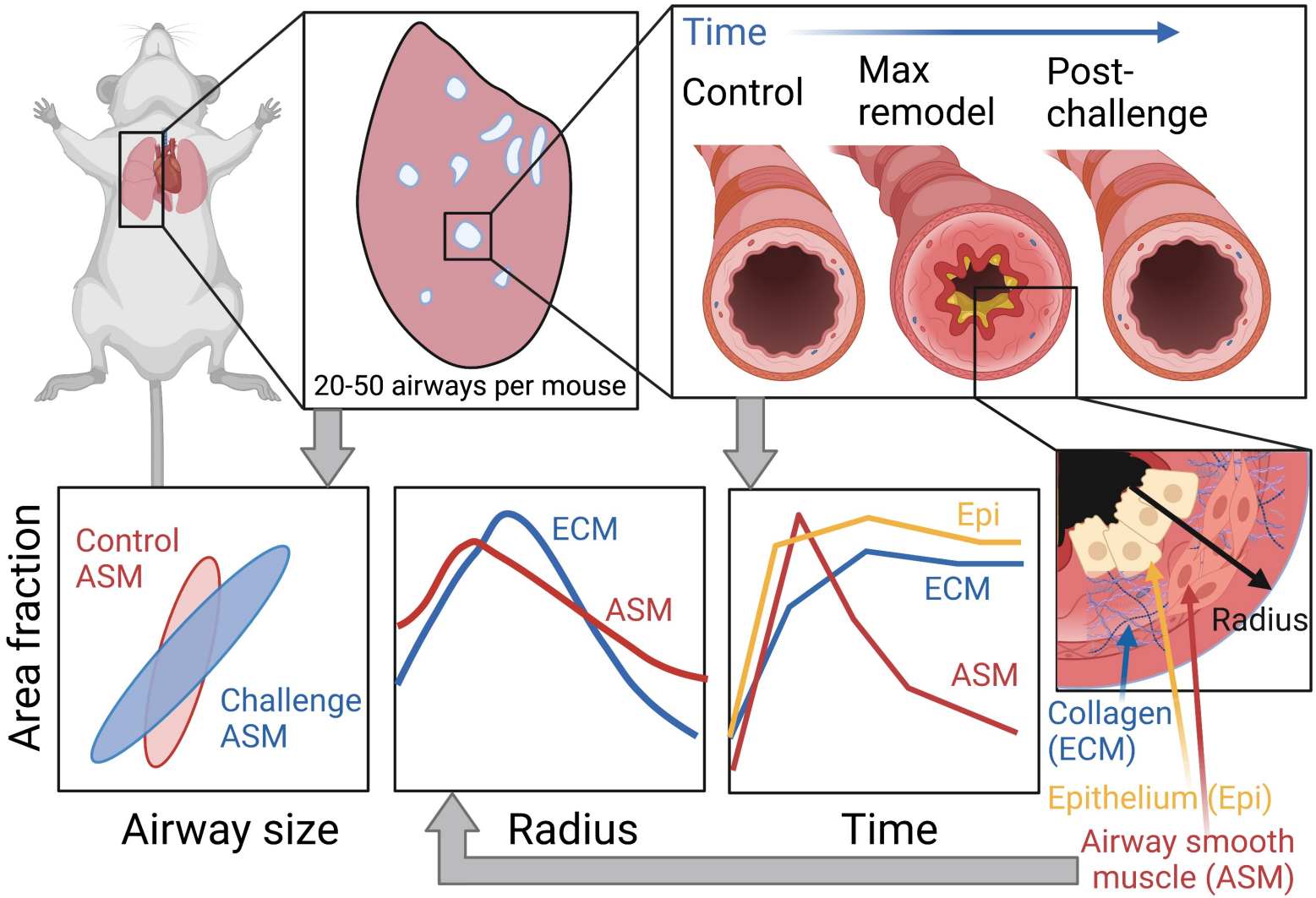

CONCLUSION

Post ovalbumin challenge, ASM changes resolved over seven days whereas ECM and epithelial changes persisted, ASM changes were greater near the basement membrane whereas ECM increase was more diffuse across the airway, and large and small airways remodelled differently.

Created with BioRender.com